Bulk and surface analysis of Hägg Fe carbide (Fe_5C_2): a density functional theory study

2008 J. Phys.: Condens. Matter 20 064238

(http://iopscience.iop.org/0953-8984/20/6/064238)

J. Phys.: Condens. Matter **20** (2008) 064238 (11pp) doi:10.1088/0953-8984/20/6/064238

Bulk and surface analysis of Hägg Fe carbide (Fe_5C_2): a density functional theory study

P J Steynberg, J A van den Berg and W Janse van Rensburg[1]

Sasol Technology (Pty) Ltd, R&D Division, 1 Klasie Havenga Road, Sasolburg 1947, South Africa

E-mail: Werner.JansevanRensburg@sasol.com

Received 29 August 2007
Published 24 January 2008
Online at stacks.iop.org/JPhysCM/20/064238

Abstract

A comprehensive density functional theory (DFT) study analysing the bulk and various low Miller index surfaces of Hägg Fe carbide (Fe_5C_2), considered to be the active phase in Fe-catalysed Fischer–Tropsch synthesis (FTS), has been carried out. The DFT determined bulk structure of Hägg Fe carbide (Fe_5C_2) is found to be in good agreement with reported monoclinic ($C2/c$) XRD data, independently of whether a monoclinic ($C2/c$) or triclinic ($P\bar{1}$) bulk structure is used as input for calculations. Attention is focused on the construction of a surface energy stability trend with subsequent correlation with particular surface properties. It is found that a (010) Miller index plane results in the most stable surface (2.468 J m^{-2}), while a (101) surface is the least stable (3.281 J m^{-2}). The systematic comparison of calculated surface energies with surface properties such as the number of dangling bonds and surface atom density (within a broken bond model), as well as unrelaxed surface energies, relative ruggedness of surfaces, degree of surface relaxation upon optimization, total spin density changes of surfaces compared to the bulk, etc, result in only an approximate correlation with the surface stability trend in selected cases. From the results it is concluded that the relative surface energies fall in a narrow range and that a large number of additional surfaces may be defined, e.g. from higher Miller index planes, sharing similar surface energy values. The results serve to demonstrate the rich complexity and diverse nature of the Fe carbide phase responsible for FTS, effectively laying the foundation for further fundamental studies.

(Some figures in this article are in colour only in the electronic version)

1. Introduction

Iron based catalysts are among the most widely used for industrial Fischer–Tropsch synthesis (FTS) of hydrocarbon products from synthesis gas ($CO + H_2$) [1, 2]. FTS is particularly suited for the production of chemicals and fuels from coal and natural gas feedstocks. Lately, the application of FTS is receiving renewed interest from both industry and academia as an alternative technology for fuel production in the light of significant increases in the cost of crude oil. During catalyst pre-treatment iron based catalysts undergo several phase transformations involving haematite (α-Fe_2O_3) conversion to magnetite (Fe_3O_4), followed by reduction to Fe metal and subsequent formation of Fe carbide phases in the presence of CO or synthesis gas [3]. An Fe carbide phase is regarded as the active state of the catalyst during FTS [4, 5]. Although several Fe carbide phases may in principle be formed, including ε-Fe_2C, ε'-$Fe_{2.2}C$, θ-Fe_3C and χ-$Fe_{2.5}C$ (Hägg Fe carbide; Fe_5C_2) it is commonly accepted that Hägg Fe carbide (Fe_5C_2) is the catalytically active Fe carbide phase for FTS [6–9]. The bulk crystal structure of Hägg Fe carbide (Fe_5C_2) was traditionally characterized to be monoclinic (space group $C2/c$) [10–13]. However, a recent re-determination of the crystal structure suggests that a formal triclinic (space group $P\bar{1}$) classification is more appropriate [14].

[1] Author to whom any correspondence should be addressed.

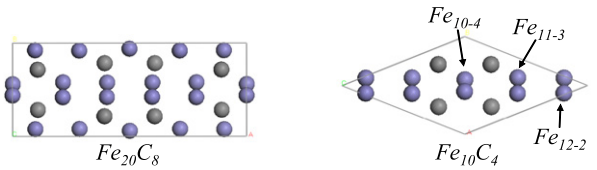

Conventional Monoclinic (*C2/c*) Primitive Monoclinic

Figure 1. Conventional ($Fe_{20}C_8$) and primitive ($Fe_{10}C_4$) representations of the monoclinic ($C2/c$) unit cell structure of bulk Hägg Fe carbide (both representations of the bulk unit cell is viewed along the *c*-axis; the blue and grey atoms refer to Fe and C, respectively).

Most reported computational studies related to Fe-catalysed FTS focus on pure Fe surfaces as model Fe catalysts. This is motivated by the availability of fundamental experimental data for pure Fe surfaces to validate computational results, as well as the simplicity of the catalyst models. In particular, a significant number of density functional theory (DFT) studies focusing on elementary FTS reactions, e.g. CO adsorption and dissociation, H_2 adsorption, methanation (CH_x) thermodynamics, etc, are reported for the Fe(100) surface [15–24] while similar DFT studies on Fe(110) [23–26] and Fe(111) [27–29] are also reported. In addition, DFT studies on the diffusion of hydrogen and carbon in bulk Fe are also reported [30, 31]. In contrast, similar DFT studies focused on Fe carbides are scarce, restricted mainly to Hägg Fe carbide (Fe_5C_2) [32–36] and cementite (Fe_3C) [36–38].

Despite the many experiments known to verify the importance of Hägg Fe carbide (Fe_5C_2) as the active catalyst phase during FTS, experimental characterization of the catalyst surface(s) is totally lacking. Furthermore, although detailed DFT studies on the adsorption behaviour of H_2 and CO on three Fe_5C_2 surfaces are available from the literature [32–34], no rationalization of the surface selections is presented. In the current paper DFT studies focused on a first systematic analysis of the bulk and selected surfaces of Hägg Fe carbide (Fe_5C_2) are presented, with the aim of correlating the calculated surface stability trend with various surface properties, similar to a reported DFT analysis on cementite (Fe_3C) [37]. It is envisaged that the results will not only provide insight into the selection of relevant Fe_5C_2 surface models for future FT mechanistic DFT studies, but will also assist in experimental characterization of active catalyst surfaces.

2. Computational details

All calculations were performed with the CASTEP periodic density functional theory (DFT) code [39] as implemented in the MaterialsStudio (Version 3.2) program package available from Accelrys Inc. Iterative solutions of the Kohn–Sham equations were performed with plane wave basis sets defined by a kinetic energy cut-off equal to 340 eV. Brillouin zone samplings were obtained from the Monkhorst–Pack scheme [40] according to *k*-point spacings of $\sim$0.05 Å^{-1} in all lattice directions, except for the surface normal directions, which employed a single *k*-point. Spin polarization was included for all calculations on the ferromagnetic Hägg Fe carbide (Fe_5C_2) systems with Gaussian smearing of 0.1 eV.

For all *bulk* calculations three different generalized gradient approximation (GGA) exchange–correlation (XC) functionals were employed for validation purposes, namely the PW91 functional of Perdew and Wang [41], the PBE functional of Perdew *et al* [42] and the revised PBE functional of Hammer, Hansen and Nørskov (termed RPBE) [43]. The Fe and C ionic cores were described by different variations of ultrasoft pseudopotentials (uspp's) [44] available in CASTEP and are explicitly noted in the text. For all bulk optimizations both the cell dimensions and fractional atomic positions were allowed to relax.

For all *surface* calculations the PBE functional was used together with the standard CASTEP ultrasoft pseudopotentials, Fe-00 and C-00, for carbon and iron cores, respectively. Periodic slab surface models, varying in thickness according to Fe_5C_2 stoichiometric units (4–16 Fe_5C_2 units were considered for all slabs), with vacuum gap spacings of 10 Å were employed. For all surface calculations the atoms representing the bulk in the slab were fixed to their fractional positions, while atoms exposed at the surface were left free to relax, taking particular care to ensure converged total energy values for the slabs with respect to degree of atom constraints in the bulk regions. The calculation of converged surface energies (E_s) with respect to slab layer thickness was not trivial for the Hägg Fe carbide surface models considered. A detailed discussion on both the calculation of converged surface energies and nature of the surface models considered are therefore presented in section 3.

3. Results and discussion

3.1. Bulk Hägg Fe carbide

The powder diffraction data and crystal structure of Hägg Fe carbide (Fe_5C_2) are well described in literature reports [10–13]. In particular, Senateur [12] and Retief [13] reported the conventional bulk unit cell to be monoclinic with space group $C2/c$ and cell dimensions: $a = 11.588$ Å, $b = 4.579$ Å, $c = 5.059$ Å, $\beta = 97.75°$. Figure 1 illustrates this conventional structure ($Fe_{20}C_8$) along with the equivalent primitive *C*-centred monoclinic representation ($Fe_{10}C_4$). All Fe atoms are 14 fold coordinated, while the C atoms are 7 fold coordinated. There are no C–C interactions in the bulk structure. The monoclinic bulk unit cell consists of three unique Fe atoms (labelled $Fe_{10\text{-}4}$, $Fe_{11\text{-}3}$ and $Fe_{12\text{-}2}$ in figure 1) and one unique C atom. The three unique Fe atoms are defined by the nature and number of its respective nearest neighbours: $Fe_{10\text{-}4}$ (10 Fe–Fe and 4 Fe–C bonds), $Fe_{11\text{-}3}$ (11 Fe–Fe and 3 Fe–C bonds) and $Fe_{12\text{-}2}$ (12 Fe–Fe and 2 Fe–C bonds).

The initial computational evaluation of bulk Hägg Fe carbide involved full atom and cell optimizations of the primitive monoclinic unit cell ($Fe_{10}C_4$) by employing different general gradient approximation (GGA) exchange–correlation (XC) functionals and core-corrected ultrasoft pseudopotential (uspp–cc) combinations for Fe and C. In particular, all three

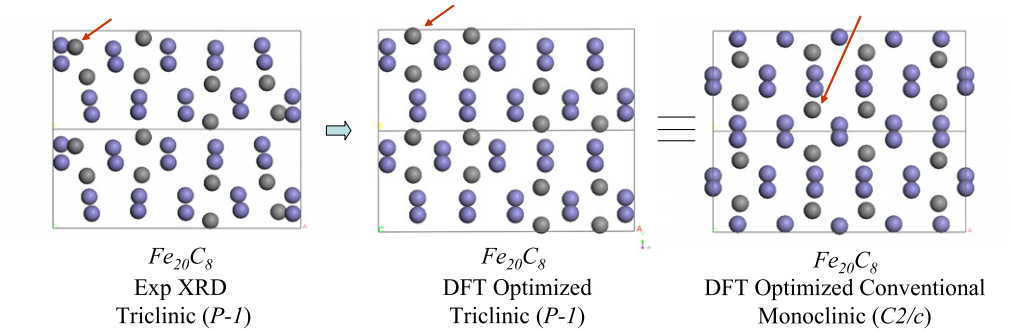

Figure 2. Illustration of experimentally determined triclinic ($P\bar{1}$), DFT optimized triclinic ($P\bar{1}$) and DFT optimized conventional monoclinic ($C2/c$) structures of bulk Hägg Fe carbide (the equivalent atom position for each of the three unit cell representations are indicated by the arrows and the structures are viewed along the c-axis; the blue and grey atoms refer to Fe and C, respectively).

Table 1. Monoclinic conventional cell parameters for Hägg Fe carbide as optimized with different GGA XC functionals and the Fe-00/C-00PBE pseudopotential combination.

Exp./XC	a (Å)	b (Å)	c (Å)	β (deg)	Error (%)[b]
Exp.[a]	11.588	4.579	5.069	97.8	—
PW91	11.510	4.477	4.952	97.6	−5.21
PBE	11.496	4.485	4.962	97.6	−4.92
RPBE	11.568	4.523	5.002	97.7	−2.62

[a] See references [12] and [13].

[b] Sum of lattice parameter percentage errors with respect to the experimental XRD data.

available GGA XC functionals in CASTEP 3.2, namely PBE, RPBE and PW91, were evaluated in combination with the two available uspp–cc's for Fe, namely Fe-00 and Fe-00PBE, and two ultrasoft pseudopotentials (uspp's) for C, namely C-00 and C-00PBE. Although both Fe-00PBE and C-00PBE uspp's are formally optimized for the PBE XC functional, all XC/uspp combinations were considered. It is found that different combinations of pseudopotentials for Fe and C essentially provide equivalent cell parameter data for a particular XC functional, with calculated lattice parameter distance differences <0.02 Å for all pseudopotential combinations considered. Table 1 summarizes representative monoclinic conventional unit cell ($Fe_{20}C_8$) parameters for the Fe-00/C-00PBE pseudopotential combination for the three XC functionals considered.

From the data presented in table 1 it is evident that for all three functionals considered the calculated lattice parameters are consistently smaller compared to the experimental values. The lattice parameter total errors calculated with PW91 and PBE are comparable at −5.21 and −4.92%, respectively, while the lattice parameter total error calculated with RPBE is significantly less at −2.62%. These results suggest that the RPBE XC functional is superior to the PW91 and PBE XC functionals in predicting the most accurate *structural* parameters for bulk Hägg Fe carbide.

In contrast to the commonly accepted monoclinic structure of Hägg Fe carbide, du Plessis, *et al* [14] recently reported that the Hägg Fe carbide structure should formally be assigned as triclinic ($P\bar{1}$ space group). Their studies involved a re-determination of unit cell atom positions and space group by simulated annealing and selected area electron diffraction (SAED), respectively, followed by improved Rietveld refined fitting to experimental powder diffraction XRD data. The determined cell dimensions of this triclinic Hägg Fe carbide structure are: $a = 11.570$ Å, $b = 4.571$ Å, $c = 5.059$ Å, $\alpha = 89.9°$, $\beta = 97.8°$ and $\gamma = 90.0°$. These cell parameters are very similar to previously reported monoclinic cell parameters, making a designation of this formally triclinic structure as *pseudo*-monoclinic appropriate. However, the atom positions in the triclinic unit cell are different compared to the atom positions of the formally monoclinic structure as is evident in figure 2.

The experimentally determined triclinic ($P\bar{1}$) Hägg Fe carbide structure was also considered as input for DFT bulk optimizations to determine whether alternative starting cell parameters and atom positions would lead to a lower energy structure which is not formally monoclinic. For these calculations the most appropriate RPBE/Fe-00/C-00PBE XC/uspp combination, as found above for monoclinic optimizations, was used. For all calculations spontaneous optimization of atom positions resembling the previously optimized conventional monoclinic unit cell structure were obtained, as illustrated in figure 2. The optimized cell parameters for this triclinic ($P\bar{1}$) starting structure are: $a = 11.580$ Å, $b = 4.530$ Å, $c = 5.003$ Å, $\alpha = 90.0°$, $\beta = 97.7°$ and $\gamma = 89.8°$, making the optimized structure also *formally* triclinic. However, this formally triclinic ($P\bar{1}$) optimized structure is only 0.04 eV (0.9 kcal mol^{-1}) per unit cell lower in energy compared to the conventional monoclinic ($C2/c$) structure optimized before, effectively suggesting that the accurate distinction of the structure as formally monoclinic or triclinic is inconclusive when the expected accuracy (∼4 kcal mol^{-1}) of the DFT calculations is kept in mind. Similar results are obtained when optimizations are performed without any symmetry constraints ($P1$).

It is particularly evident, however, that the DFT optimized position for one carbon atom deviates appreciably from the experimentally determined position for the triclinic structure, while agreement with the experimental monoclinic structure is particularly good. One possible explanation for this discrepancy may be that the higher symmetry monoclinic ($C2/c$) structure should be regarded as an average structure

of the extended bulk in which the lower symmetry triclinic ($P\bar{1}$) structure is present in different orientations in different unit cells. In an effort to assess this possibility supercell bulk geometries were constructed as input for calculations from the experimental triclinic ($P\bar{1}$) structure. Each of the experimental triclinic ($P\bar{1}$; $Fe_{20}C_8$) cell dimensions ($a = 11.570$ Å, $b = 4.571$ Å, $c = 5.059$ Å) was doubled to yield three new supercell ($Fe_{40}C_{16}$) input structures with dimensions $(2a)bc$, $a(2b)c$ and ab $(2c)$, respectively. However, the optimization of the atom positions for these supercells all resulted in relative positions resembling the originally optimized monoclinic ($C2/c$) structure. Further unit cell enlargement to $Fe_{80}C_{32}$ supercell structures with dimensions $(2a)(2b)c$, $(2a)b$ $(2c)$ and a $(2b)(2c)$ and $Fe_{160}C_{64}$ supercell structures with dimensions $(2a)(2b)(2c)$ and a $(2b)(4c)$ also resulted in optimized atom positions resembling the monoclinic ($C2/c$) bulk structure. From these results it is thus concluded that a monoclinic ($C2/c$) structure for bulk Hägg Fe carbide is recognized from the DFT optimizations in agreement with earlier experimental structure determinations. Therefore, the theoretical cleavage of Hägg Fe carbide surfaces will be performed on a monoclinic bulk structure (*vide infra*).

In the discussion thus far correlation of calculated *structural* data for bulk Hägg Fe carbide was compared with available experimental data. In an effort to validate the calculation of *electronic* properties of the bulk structure, the magnetic moment of the ferromagnetic bulk Hägg Fe carbide was considered. The only experimentally available magnetic moment data for bulk Hägg Fe carbide, i.e. averaged over the Fe atoms, was determined by saturation magnetization experiments to fall in a range of 1.72–1.75 μ_B [45]. In the current study the magnetic moment for primitive monoclinic ($C2/c$; $Fe_{10}C_4$) bulk Hägg Fe carbide was calculated from the site-projected spin partial density of states (PDOS) by obtaining the total spin difference in the site-projected PDOS integrated up to the Fermi level, similar to the approach described by Chiou and Carter [37] for calculating the magnetic moment of cementite (Fe_3C). This approach allows for the calculation of local magnetic moments on specific atoms in the bulk in addition to an average magnetic moment for the total bulk. The magnetic moments for Hägg Fe carbide, averaged over the number of Fe atoms, as calculated with PW91, PBE and RPBE are 1.70, 1.76 and 1.83 μ_B, respectively. A comparison of these magnetic moment values with the experimental values (1.72–1.75 μ_B) reveals that the PW91- and PBE determined values are in good agreement, while an overestimation is calculated with RPBE. Further analysis of the PBE-calculated localized magnetic moment on the different Fe atoms in the primitive bulk shows significant differences in *local* magnetic moments for $Fe_{10\text{-}4}$ (1.07 μ_B), $Fe_{11\text{-}3}$ (1.72 μ_B) and $Fe_{12\text{-}2}$ (2.15μ_B) suggesting distinct differences in electronic nature of the different Fe atoms in the bulk (see figure 1 for distinction of Fe atoms). It is also interesting to note that the local magnetic moment calculated with PBE for C in primitive bulk Hägg Fe carbide is -0.20 μ_B, effectively suggesting a spin density slightly deviating from zero and of opposite spin compared to the Fe atoms. A similar result was reported for the magnetic moment of C in bulk cementite (Fe_3C) [37].

Table 2. Table of unique and equivalent low Miller index planes that may theoretically be cleaved from the conventional monoclinic bulk structure of Hägg Fe carbide ($Fe_{20}C_8$).

Unique low Miller index	Equivalent Miller index
(001)	$(00\bar{1})$
(010)	$(0\bar{1}0)$
(100)	$(\bar{1}00)$
(101)	$(\bar{1}0\bar{1})$
(110)	$(\bar{1}10)$, $(1\bar{1}0)$, $(\bar{1}\bar{1}0)$
(011)	$(0\bar{1}1)$, $(01\bar{1})$, $(0\bar{1}\bar{1})$
(111)	$(\bar{1}\bar{1}1)$, $(\bar{1}1\bar{1})$[a], $(1\bar{1}1)$[a]
$(11\bar{1})$	$(\bar{1}\bar{1}1)$, $(1\bar{1}\bar{1})$[b], $(\bar{1}11)$[b]
$(10\bar{1})$	$(\bar{1}01)$

[a] Equivalent to (111) cleaved at 0.5 fractional distance from bulk origin.

[b] Equivalent to $(11\bar{1})$ cleaved at 0.5 fractional distance from bulk origin.

3.2. Surfaces of Hägg Fe carbide

The focus of the current study is to theoretically cleave a series of surfaces from the bulk structure of Hägg Fe carbide with subsequent comparison of calculated surface energies. However, the strategy for cleaving low Miller index surfaces is not trivial, because a large number of surfaces may essentially be generated. Consequently, the strategy adopted in the current study follows the following rules, effectively ensuring a systematic surface analysis: (i) only low Miller index surfaces are considered, i.e. the Miller index numbers consist only of 0 and/or 1 and/or -1. (ii) The slabs cleaved are stoichiometric to the bulk, i.e. the slab stoichiometry $= n \times Fe_5C_2$. (iii) The slabs are symmetric, i.e. the top and the bottom faces of the slabs are equivalent. In theory 26 low Miller index planes may be cleaved from the conventional monoclinic bulk structure of Hägg Fe carbide ($Fe_{20}C_8$) for (i) above. Careful comparison of these 26 low Miller index planes reveals that only 9 unique Miller indexes are necessary to describe all 26 possible planes. These 9 unique Miller indexes are listed in table 2 along with the corresponding equivalent Miller indexes (17 in total), to yield a total of 26 Miller indexes.

For all 9 unique Miller indexes listed in table 2, slabs which are both *stoichiometric*and *symmetric* may be cleaved. For 5 of the 9 Miller indexes, i.e. excluding (001), (100), (101) and $(10\bar{1})$, two unique surfaces, which are both stoichiometric and symmetric, can be cleaved which in turn depends on the fractional position of cleavage through the bulk (*vide infra*). This effectively accounts for a total of 14 unique stoichiometric and symmetric surfaces that could successfully be identified upon cleavage from the bulk.

As an example, the two relevant slabs for the (110) Miller plane are presented in figure 3. Stoichiometric and symmetric cleavage of bulk Hägg Fe carbide proceeds by cleaving either through the origin (Slab A) of the conventional bulk unit cell or at a 0.5 fractional distance along both the a- and b-axes (Slab B). The nomenclature used to distinguish the slabs is (110) 0.00 and (110) 0.50, respectively. This nomenclature will be used throughout the remainder of this paper to distinguish between different surfaces generated from

Table 3. Calculation of surface energies (E_s) with increase in slab thickness for two Hägg Fe carbide surfaces, namely (110) 0.00 and (111) 0.00, by either directly calculating E_b (Method 1) or calculation E_b according to the Boettger method (Method 2) [46].

	(110) 0.00			(111) 0.00		
	E_s (J m^{-2})			E_s (J m^{-2})		
Slab	Thickness (Å)[a]	Method 1[b]	Method 2[c]	Thickness (Å)[a]	Method 1[b]	Method 2[c]
$Fe_{20}C_8$	7.3	2.717	—	5.5	2.800	—
$Fe_{30}C_{12}$	12.2	2.724	2.709	8.6	2.812	2.780
$Fe_{40}C_{16}$	16.4	2.724	2.704	11.7	2.820	2.778
$Fe_{50}C_{20}$	20.5	2.731	2.706	14.8	2.828	2.775
$Fe_{60}C_{24}$	24.7	2.737	2.707	17.9	2.842	2.779

[a] Thickness of the respective slabs.
[b] E_s calculated with E_b directly calculated from the primitive bulk structure of Hägg Fe carbide.
[c] E_s calculated with E_b determined according to the Boettger method [46].

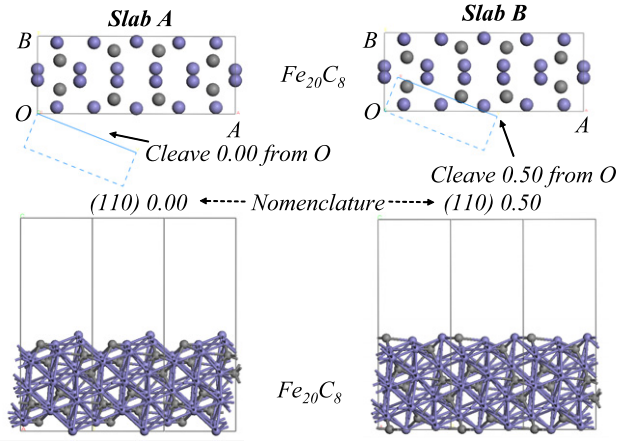

Figure 3. Example of the two possible stoichiometric and symmetric slabs that may be cleaved from conventional bulk Hägg Fe carbide ($Fe_{20}C_8$) for the (110) Miller index (unit cells are viewed along the *b*-axis; the blue and grey atoms refer to Fe and C, respectively).

similar Miller indexes. It should be noted that no additional (110) slabs can be cleaved satisfying both the stoichiometry and symmetry requirements.

For all surface optimizations careful validation of the appropriate calculation parameters, including XC functional, cut-off energy, *k*-point sampling, vacuum gap spacing and degree of bulk region constraints, with respect to surface energy were performed. For all surface energies reported here, PBE optimized structures and energies were calculated with 340 eV cut-off, *k*-point spacings of ∼0.05 Å^{-1} (for the *a*- and *b*-axes of the surface unit cells), 10 Å vacuum gaps and frozen atoms in the centre of the slabs with all surface atoms exposed on both the top and the bottom faces allowed to freely relax. However, the convergence of calculated surface energies with respect to increasing slab thicknesses were not trivial and will be further discussed here.

The calculation of surface energies (E_s) explicitly incorporates the total energy of the bulk (E_b) from which the respective surfaces are cleaved according to the following general expression:

$$E_s = \frac{(E_n - nE_b)}{2A}$$

where E_n refers to the total energy of the slab containing n bulk units (in the case of Hägg Fe carbide $n = 1$ refers to one primitive monoclinic bulk unit of stoichiometry $Fe_{10}C_4$) and A is the surface area of the surface unit cell. Essentially two methods may be used to calculate E_b, Method 1: calculation of E_b by optimization of a suitable bulk unit cell (most commonly used) and Method 2: calculation of E_n for at least two values of n followed by determination of $E_b = E_{n+1} - E_n$ (also referred to as the Boettger method [46]). In the current studies it is found that calculation of Hägg Fe carbide surface energies (E_s) by estimating E_b from Method 1 results in computationally divergent values for E_s as n increases, i.e. with increasing slab thickness. Method 1 does have the advantage, however, of requiring only one slab optimization to obtain E_s. Although the Boettger method (Method 2) does not require a bulk optimization, it has the disadvantage of requiring multiple slab calculations. However, the calculation of Hägg Fe carbide surface energies with the Boettger method does converge quite rapidly with increasing n.

The application of these methods is best illustrated by e.g. the calculation of the surface energies for Hägg Fe carbide surfaces (110) 0.00 and (111) 0.00 with increasing slab thickness (table 3). In both cases the increase in slab thickness is correlated to increase in slab stoichiometry in increments of $Fe_{10}C_4$. From table 3 it is evident that diverging surface energies with increasing slab thickness are obtained for both (110) 0.00 and (111) 0.00 when the bulk energy (E_b) is directly calculated from the primitive monoclinic Hägg Fe carbide bulk structure (Method 1). However, rapid convergence of surface energies with increasing slab thickness are obtained by application of the Boettger method to determine E_b. It should also be noted that the values for E_s are greater for Method 1 compared to Method 2 (Boettger method).

The appropriate use of the Boettger method requires the optimization of a series of slabs with increasing thickness with at least three consecutive slab thicknesses required for determining E_s convergence. A further advantage of the Boettger method is that the error associated with a converged calculated surface energy value may easily be determined by e.g. standard deviations. Accordingly, the calculation of converged surface energies with respect to increased slab thickness for all 14 low Miller index surface models identified in the current study (*vide supra*) were determined

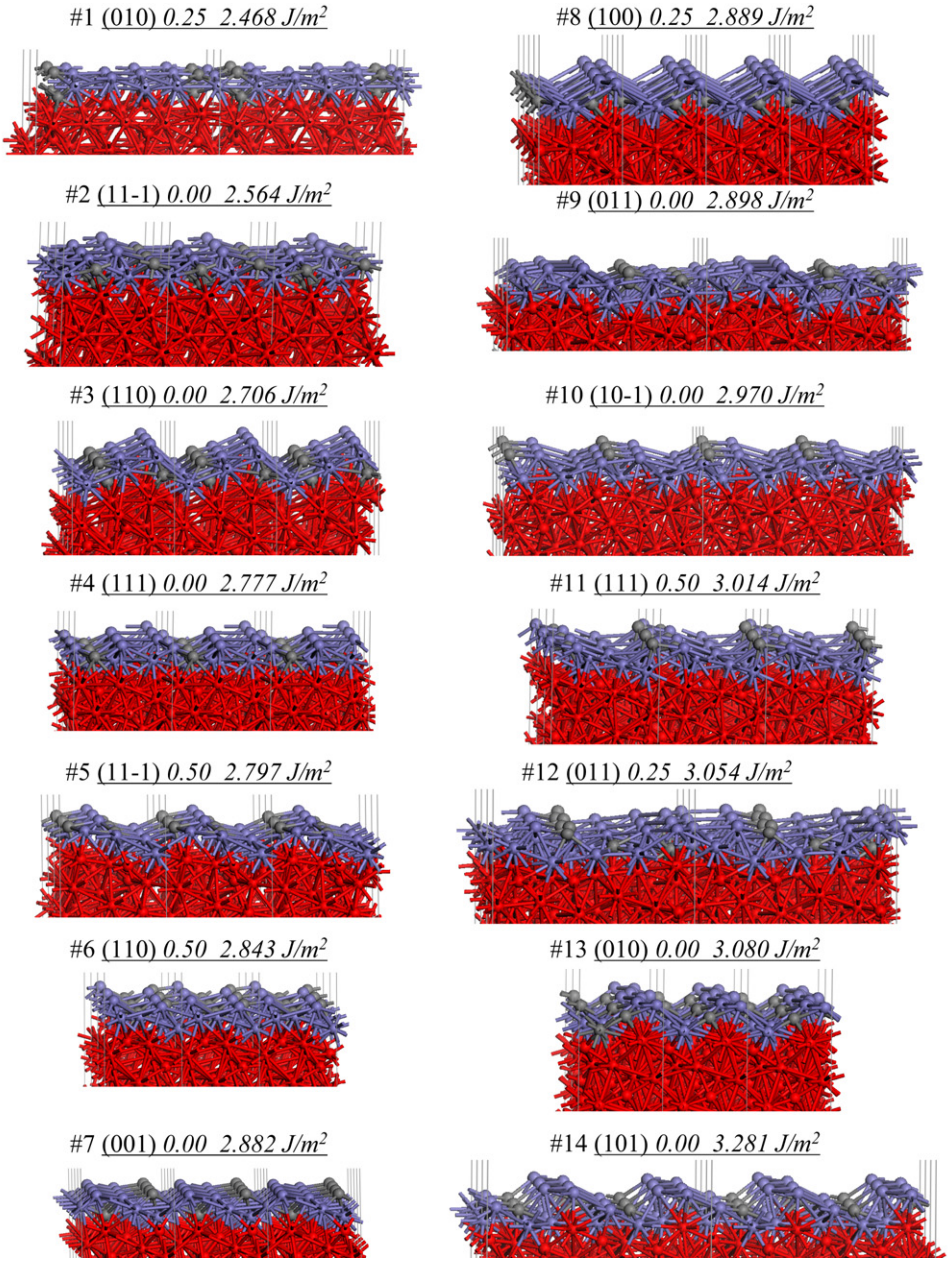

Figure 4. Cross-sections of optimized geometries and surface energies ($E_{s,rel}$ in J m^{-2}) for all stoichiometric and symmetric low Miller index Hägg Fe carbide surfaces considered in the current study (only the surface regions of the slabs are shown; the blue and grey atoms refer to Fe and C, respectively, while the atoms coloured in red were fixed to bulk optimized fractional positions during slab optimization).

by application of the Boettger method. Figure 4 illustrates the optimized geometries and relaxed surface energies ($E_{s,rel}$ in J m^{-2}) for all 14 stoichiometric and symmetric low Miller index Hägg Fe carbide surfaces considered. Additional surface properties and calculated data are summarized in table 4.

In table 4 the *surface properties* as cleaved from the conventional bulk structure of Hägg Fe carbide are summarized, including surface unit cell lattice vectors (u and v in Å), surface unit cell areas (A in Å^2), the number of bonds broken to generate the surface atoms per unit cell surface area (dangling bonds/Å^2) and the surface atom density (surface atoms/Å^2). Previously it was mentioned (*vide supra*) that each Fe and C in bulk Hägg Fe carbide contains 14 and 7 nearest neighbours, respectively, as defined for nearest neighbour atoms closer than 2.700 and 2.300 Å for Fe–Fe and Fe–C distances, respectively. Therefore, the number of dangling bonds for each surface unit cell slab is obtained by calculating the total number of bonds broken for each surface Fe (i.e. total number of bonds less than 14 per surface Fe) and surface carbon (i.e. total number of bonds less than 7 per surface C) in the respective surface unit cells. Similarly, a surface atom is defined as any atom on the surface having at least one nearest neighbour less than 14 for Fe and at least one nearest neighbour less than 7 for C. From the surface unit cell dimensions listed in table 4 it is evident that significant differences in both lattice vector lengths and surface areas exist for the 14 slabs studied. In particular, the surface unit cell areas span a significant range from 22.2 to 76.3 Å^2.

Table 4. Table analysing the properties of low Miller index Hägg Fe carbide surfaces.

		Surface Properties[a]						Calculated surface energy data[a]					Surface optimization data[a]		
Entry	Surface	u (Å)	v (Å)	θ (deg)	A (Å^2)	Dangling bonds (Bonds Å^{-2})	Surf density (Atoms Å^{-2})	$E_{s,unrel}$ (J m^{-2})	$E_{s,rel}$ (J m^{-2})	ΔE_s (J m^{-2})	ΔE_s (%)	$E_{s,surf}$ (kJ mol^{-1})	rms relax (10^{-3} Å)	rms relax/A (10^{-3} Å^{-1})	z-relax (10^{-3} Å)
1	(010) 0.25	4.951	11.493	97.6	56.4	0.851	0.248	2.812	2.468	0.344	12.2	59.9	91	1.61	351
2	(11$\bar{1}$) 0.00	6.673	6.166	109.5	38.8	0.722	0.232	2.742	2.564	0.177	6.5	66.5	66	1.69	113
3	(110) 0.00	4.951	6.166	97.1	30.3	0.825	0.231	3.274	2.706	0.568	17.3	70.5	76	2.51	87
4	(111) 0.00	6.166	6.673	98.8	40.7	0.787	0.246	2.972	2.777	0.195	6.6	68.0	85	2.09	141
5	(11$\bar{1}$) 0.50	6.673	6.166	109.5	38.8	0.774	0.232	3.045	2.797	0.248	8.1	72.6	104	2.68	144
6	(110) 0.50	4.951	6.166	97.1	30.3	0.825	0.264	3.164	2.843	0.321	10.1	64.8	109	3.60	183
7	(001) 0.00	6.167	4.475	111.3	25.7	0.739	0.233	3.178	2.882	0.296	9.3	74.4	98	3.80	143
8	(100) 0.25	4.475	4.951	90.0	22.2	0.813	0.271	2.965	2.889	0.076	2.6	64.2	50	2.25	70
9	(011) 0.00	11.493	6.673	84.4	76.3	0.799	0.223	3.210	2.898	0.312	9.7	78.4	112	1.47	289
10	(10$\bar{1}$) 0.00	4.475	11.900	90.0	53.2	0.657	0.225	3.283	2.970	0.313	9.5	79.4	127	2.38	212
11	(111) 0.50	6.166	6.673	98.8	40.7	0.836	0.246	3.377	3.014	0.363	10.7	73.8	115	2.82	189
12	(011) 0.25	11.493	6.673	84.4	76.3	0.812	0.236	3.553	3.054	0.499	14.0	78.0	125	1.63	198
13	(010) 0.00	4.951	11.493	97.6	56.4	0.851	0.284	3.368	3.080	0.287	8.5	74.7	109	1.93	168
14	(101) 0.00	13.099	4.475	90.0	58.6	0.887	0.273	3.482	3.281	0.201	5.8	72.4	112	1.90	155

[a] See text for the definition of properties and calculated data summarized in this table.

This necessitates the normalization of surface properties with respect to unit cell surface area, such as the number of dangling bonds and number of surface atoms, to enable potential correlation with the calculated surface energy stability trend (*vide infra*).

The numbering sequence used for the surfaces in figure 4 and table 4 corresponds to an increasing surface energy trend as calculated from the relaxed slabs, i.e. $E_{s,rel}$. The calculated values for $E_{s,rel}$ span a range from 2.468 J m^{-2} for the most stable surface, (010) 0.25, to 3.281 J m^{-2} for the least stable surface in the series, (101) 0.00. It is also evident that different surfaces cleaved from the same Miller index plane could exhibit distinctly different surface energies, as is e.g. observed for (010) 0.25 (2.468 J m^{-2}) versus (010) 0.00 (3.080 J m^{-2}) which occupy the 1st and 13th respective positions on the surface stability trend. From the optimized geometries of the relaxed surfaces illustrated in figure 4 the large variation of surface atom structural compositions for the respective surfaces are clear. However, a direct correlation of the surface structures with the calculated surface stability trend is not instantly recognizable from visual inspection. It may, however, be pointed out that the flattest (terrace) surfaces, such as (010) 0.25 and (11$\bar{1}$) 0.00, are calculated to have the lowest $E_{s,rel}$ values, while the most rugged (uneven) surfaces, such as (010) 0.00 and (101) 0.00, have the highest calculated $E_{s,rel}$ values. This rather imprecise definition is, however, not applicable in all instances, as is evident from the relatively low surface energy of the stepped (110) 0.00 (2.706 J m^{-2}) surface compared to the relatively flatter (011) 0.00 (2.898 J m^{-2}) surface.

The calculation of surface energies for the unrelaxed slabs ($E_{s,unrel}$) was also conducted to: (i) provide a basis for determination of the degree of relaxation of surface atoms during optimization, but more importantly to (ii) assess whether relative calculated surface energies may directly be correlated to the way the bulk structure is cleaved. Figure 5 plots the correlation of $E_{s,rel}$ versus $E_{s,unrel}$ for all low Miller index surfaces considered. From the graph it is evident that an approximate correlation between unrelaxed and relaxed surface energies does exist, but calculated variations in surface energy decreases ($\Delta E_s = \Delta E_{s,unrel} - \Delta E_{s,rel}$; table 4) for different surfaces upon relaxation make the use of $E_{s,unrel}$ unreliable for construction of an accurate surface energy stability trend. In particular, from table 4 it follows that ΔE_s for (110) 0.00 is 0.568 J m^{-2}, which represents a 17.3% lowering in surface energy upon surface relaxation. In contrast, for (100) 0.25 ΔE_s is only 0.076 J m^{-2} representing only a 2.6% lowering in surface energy upon relaxation.

Additional *surface optimization data* is summarized in table 4. This include the root mean square relaxation (rms relax) as the difference in atomic positions before and after optimization,

$$\text{rms relax} = \left[\frac{1}{N}\sum_{i=1}^{N}(\mathbf{r}_{i0} - \mathbf{r}_i)^2\right]^{1/2}$$

where $\mathbf{r}_{i0}$ and $\mathbf{r}_i$ refer to the unrelaxed and relaxed atomic position vectors for all atoms in representative slabs, while

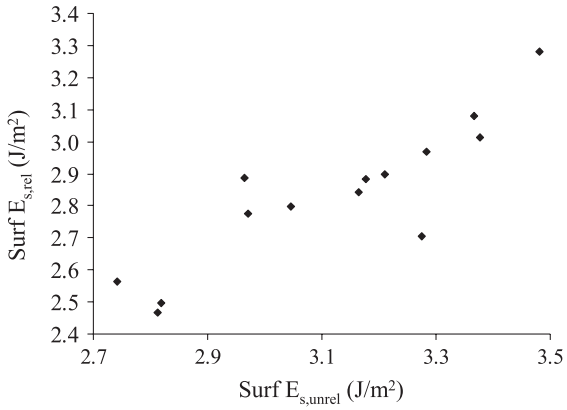

Figure 5. Graph of relaxed surface energies ($E_{s,rel}$) versus unrelaxed surface energies ($E_{s,unrel}$) for the 14 low Miller index surfaces cleaved from bulk Hägg Fe carbide.

rms relax/A is rms relax normalized to surface area. The z-relax parameter refers to the structural relaxation in the surface normal direction of the atom closest to the surface for each slab considered. However, despite the significant variations calculated for these three parameters among the different surfaces no correlations of any significance with calculated $E_{s,rel}$ and $E_{s,unrel}$ were found. Similar to this result no notable correlations of surface area normalized dangling bonds and surface atom densities with respect to $E_{s,unrel}$ were found, despite the approximate correlation of $E_{s,unrel}$ to the $E_{s,rel}$ stability trend. It is thus concluded that the surface stability trend summarized in figure 4 and table 4 cannot simply be correlated to either the relaxation behaviour of the surface or a simple broken bond model in isolation, but is more likely to at least involve an intricate combination of these surface *structural* features. It should be noted that formal reconstruction leading to more prominent structural changes of the surfaces was not considered in the current study.

In addition, it is conceivable that a proper evaluation of the calculated surface energy stability trend necessarily also requires the incorporation of some *electronic* properties of the surfaces slabs. In particular, this requires an analysis of some electronic properties of specific atoms (not only differences between C and Fe, but also differences between different types of Fe atoms) on the surfaces and how it is different from atoms in the bulk. In the current study one aspect of the electronic properties of selected surfaces involved the calculation of atom spin densities localized on surface atoms. For this purpose 6 surfaces were selected from the set of 14 in table 4, namely #1 (010) 0.25, #2 (11$\bar{1}$) 0.00, #4 (111) 0.00, #8 (100) 0.25, #13 (010) 0.00 and #14 (101) 0.00, effectively representing an even spread of surfaces over the calculated surface energy ($E_{s,rel}$) range of 2.486 to 3.281 J m^{-2}. For each of these surfaces the nature of the atoms exposed on the surface was identified, i.e. $Fe_{10\text{-}4}$, $Fe_{11\text{-}3}$, $Fe_{12\text{-}2}$ or C, according to its original position in the bulk structure of Hägg Fe carbide (figure 1). This was followed by the calculation of the localized atom spin by considering the spin difference in the site-projected spin PDOS integrated up to the Fermi level as illustrated in figure 6.

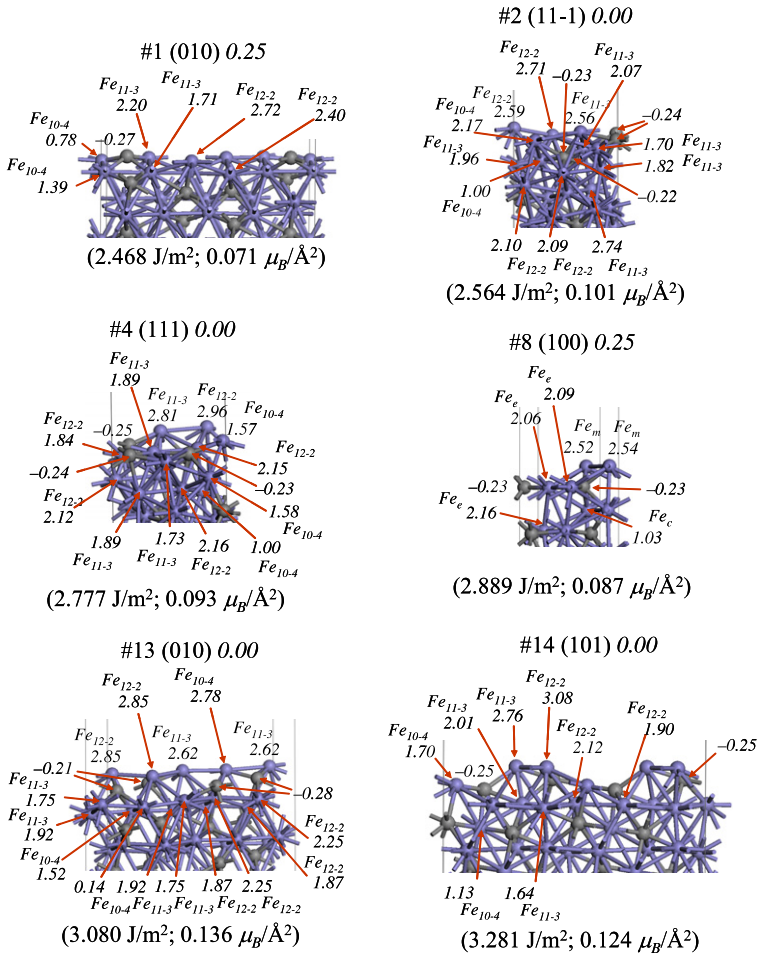

Figure 6. Analysis of localized spin densities and total normalized absolute spin density difference ($\mu_{B,total}$) for selected low Miller Hägg Fe carbide surfaces (the blue and grey atoms refer to Fe and C, respectively). Please refer to the electronic version of this paper for colour designations.

It was noted before that the calculated local spin densities for $Fe_{10\text{-}4}$, $Fe_{11\text{-}3}$ and $Fe_{12\text{-}2}$ are significantly different in bulk Hägg Fe carbide (figure 1), making it interesting to investigate the *change* in localized spin densities for these atoms upon exposure as unsaturated atoms on surfaces. For the most stable surface (010) 0.25 four of each $Fe_{10\text{-}4}$, $Fe_{11\text{-}3}$ and $Fe_{12\text{-}2}$ are exposed on the surface, together with two surface C's, per surface unit cell (due to symmetry on this surface only half of the surface atoms is labelled in figure 6). In particular, the two surface $Fe_{10\text{-}4}$ atoms is calculated to have spin densities of 0.78 and 1.39 μ_B which are both lower and higher than the spin density of $Fe_{10\text{-}4}$ (1.07 μ_B) in the bulk. A similar result is found for the surface $Fe_{11\text{-}3}$ atoms having spin densities of 1.71 and 2.20 μ_B compared to 1.72 μ_B for bulk $Fe_{11\text{-}3}$. For the two surface $Fe_{12\text{-}2}$ atoms indicated the calculated spin densities of 2.40 and 2.72 μ_B are both larger than for bulk $Fe_{12\text{-}2}$ (2.15 μ_B). For surface C a spin density of -0.27 μ_B is calculated, pointing to opposite excess spin on C compared to Fe, and a slight increase of spin density compared to bulk C (-0.20 μ_B). Analysis of localized spin densities for subsurface atoms (not indicated) essentially leads to values similar to the bulk. Similar results as presented here for (010) 0.25 are presented for the remaining five surfaces in figure 6.

If one considers the localized spin densities for atoms in bulk Hägg Fe carbide to resemble the lowest energy spin states for the respective atoms, it is possible to calculate the total deviation of local surface atom spin densities from the ideal bulk as the surface area normalized absolute spin difference ($\Delta\mu_{B,total}$) between surface and bulk atoms according to the following expression:

$$\Delta\mu_{B,total} = \frac{1}{A}\left[\sum_{i=1}^{k}\left|\mu_{Fe_{10\text{-}4},i} - \mu_{Fe_{10\text{-}4},bulk}\right| + \sum_{i=1}^{l}\left|\mu_{Fe_{11\text{-}3},i} - \mu_{Fe_{11\text{-}3},bulk}\right| + \sum_{i=1}^{m}\left|\mu_{Fe_{12\text{-}2},i} - \mu_{Fe_{12\text{-}2},bulk}\right| + \sum_{i=1}^{n}\left|\mu_{C,i} - \mu_{C,bulk}\right|\right]$$

where A is the surface unit cell area; k, l, m and n are the total number of respective $Fe_{10\text{-}4}$, $Fe_{11\text{-}3}$, $Fe_{12\text{-}2}$ and C atoms in the slab and $\mu_{Fe_{10\text{-}4}}$, $\mu_{Fe_{11\text{-}3}}$, $\mu_{Fe_{12\text{-}4}}$, μ_C are the localized spin densities on the respective atoms either in the slab or in the bulk. The calculated values for $\Delta\mu_{B,total}$ for the respective surfaces are also listed in figure 6.

For the most stable (010) 0.25 surface the calculated value for $\Delta\mu_{B,total}$ is 0.071 μ_B Å^{-2}. In contrast the calculated

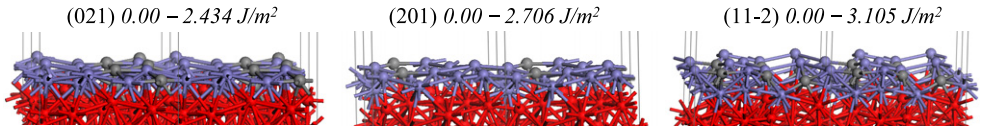

Figure 7. Optimized geometries and surface energies ($E_{s,rel}$) calculated for three random higher Miller index surfaces (only the surface regions of the slabs are shown; the blue and grey atoms refer to Fe and C, respectively, while the atoms coloured in red were fixed to bulk optimized fractional positions during slab optimization). Please refer to the electronic version of this paper for colour designations.

values of $\Delta\mu_{B,total}$ for the two least stable surfaces, (010) 0.00 and (101) 0.00, are significantly higher at 0.136 and 0.124 μ_B Å^{-2}, respectively. This suggests that the larger the deviation in total atom spin density for a cleaved surface compared to the ideal total bulk spin density, the larger the expected surface energy ($E_{s,rel}$) would be. Consequently, an approximate correlation of the calculated surface stability trend may be made with $\Delta\mu_{B,total}$, as is further evident from the intermediate $\Delta\mu_{B,total}$ values of 0.101, 0.093 and 0.087 μ_B Å^{-2} calculated for the intermediately stable (11$\bar{1}$) 0.00, (111) 0.00 and (100) 0.25 respective surfaces. Once again, however, the calculation of $\Delta\mu_{B,total}$ values are not sufficient in isolation to establish *accurate* surface stability trends, as exemplified by the erroneous ordering of the stabilities of (11$\bar{1}$) 0.00, (111) 0.00 and (100) 0.25 based on $\Delta\mu_{B,total}$ values. Nevertheless, the methodology described here may possibly be used in the approximate prediction of relative surface energies where the calculation of E_s is impossible from conventional methods, e.g. for cases where either the generation of *symmetric* or *stoichiometric* slabs from the bulk is impossible.

Lastly, it should be noted that an alternative expression for calculated surface energies, $E_{s,surf}$, is also listed in table 4 for all 14 surfaces studied. The calculation of $E_{s,surf}$ involves the normalization of surface energies with respect to mole surface atoms present for each slab to yield the unit of kJ mol^{-1}. This is different from $E_{s,rel}$ for which the normalization of surface energy is based on the area of the surface unit cells. Both these methods for calculation of surface energies are not ideal, because $E_{s,rel}$ is only correlated to the macroscopic surface unit cell areas which may deviate from actual microscopic surface areas for slabs in which significant steps (or of rugged nature) are present, while $E_{s,surf}$ depends on the convention followed for the definition of a surface atom. This reasoning also explains the different surface stability trend calculated for $E_{s,surf}$ compared to $E_{s,rel}$. However, it is interesting to note that the lowest energy surface, (010) 0.25, is recognized as such by both $E_{s,rel}$ and $E_{s,surf}$. More importantly, however, the values calculated for $E_{s,surf}$ span a range of ∼20 kJ mol^{-1}, which is close to the limit of the expected error for the DFT approach followed in this study. This effectively shows that these surfaces cleaved from bulk Hägg Fe carbide all exhibit surface energies in a very narrow range, making the selection of the most stable or most appropriate surface for catalysis not straightforward. Instead, it should rather be concluded that a large number of different Hägg Fe carbide surfaces, in addition to the surfaces considered in the current study, are likely to share the same surface energies, making a variety of different surfaces share the importance of representing the 'active catalyst' for e.g. Fischer–Tropsch synthesis. To emphasize this conclusion three randomly selected stoichiometric and symmetric higher Miller index surfaces, (021) 0.00, (201) 0.00 and (11$\bar{2}$) 0.00, were cleaved from bulk Hägg Fe carbide, optimized and surface energies calculated as illustrated in figure 7. For these random three surfaces a surface energy range from 2.434 to 3.105 J m^{-2} is obtained, essentially mirroring the surface energy range of 2.468 to 3.281 J m^{-2} (figure 4) calculated for the 14 low Miller index surfaces considered in the current study. This confirms the conclusion made above that a large number of Hägg Fe carbide surfaces are likely to share similar surface energies and may thus also be important as model surfaces for actual catalysts.

4. Conclusions

In the current study a detailed analysis of both bulk and surface properties of Hägg Fe carbide (Fe_5C_2) has been performed with DFT calculations. Hägg Fe carbide is an important Fe carbide phase active for Fe-catalysed Fischer–Tropsch synthesis (FTS). Although the bulk structure of Hägg Fe carbide is well characterized from XRD analyses, no experimental characterization of Hägg Fe carbide surfaces are available, making the choice of appropriate surface models for elementary Fischer–Tropsch mechanistic studies with DFT challenging. Consequently, a theoretical analysis of a surface stability trend for Hägg Fe carbide will be useful for not only surface model selections, but also for potential synergy with experimental surface analysis studies.

In particular, a series of 14 low Miller index surfaces was cleaved from the validated bulk structure of Hägg Fe carbide, optimized and surface energies calculated. It is shown that the calculation of converged surface energies with respect to surface layer thickness is not trivial, requiring appropriate application of the Boettger method [46]. The most stable low Miller index surface identified is (010) 0.25, while the least stable surface is (101) 0.00. In addition, the determination of various relative surface properties, including number of dangling bonds, surface atom density, unrelaxed surface energies, degree of surface energy change upon surface relaxation, degree of structural relaxation and change in total surface spin densities compared to bulk spin density, are presented and discussed. Attempts are made to correlate the calculated surface stability trend with a particular surface property or combinations thereof. However, only approximate correlations with e.g. unrelaxed surface energies, degree of surface ruggedness and total spin density changes are observed.

From these results it is concluded that an accurate correlation of surface properties with optimized surface

energies is not possible. The DFT results show that a large number of Hägg Fe carbide surfaces are likely to share similar surface energies spanning a narrow range, effectively making efforts to identify the most representative 'active' FT catalyst surface inappropriate. This conclusion is supported from surface energy data calculated for random higher Miller index surfaces. The study also demonstrates that caution is needed when random selections of Hägg Fe carbide surface models are made for DFT studies of elementary FT mechanistic steps [32–34]. Nevertheless, this study did reveal the rich complexity and diverse nature of the most likely Fe carbide phase responsible for commercial Fe-catalysed FTS, laying the foundation for both further DFT studies and experimental fundamental studies.

Acknowledgments

We acknowledge Professor Rutger van Santen (Eindhoven University), Professor Hans Niemantsverdriet (Eindhoven University), Dr Tracy Bromfield (Sasol Technology R&D), Dr Esna du Plessis (Sasol Technology R&D), Professor Eric van Steen (University of Cape Town), Mr Pieter van Helden (University of Cape Town), Dr Daniel Curulla-Ferré (Eindhoven University), Dr Ionel Ciobîca (Sasol Technology R&D), Dr Melissa Petersen (Sasol Technology R&D) and the other members of the FT Molecular Modelling Study Team for valuable discussions. We also acknowledge Mr Ivan Bester (Information Management, Sasol) for infrastructure support to the Sasol Molecular Modelling Group, and Sasol Technology Research and Development for the permission to publish this work.

References

[1] Steynberg A P and Dry M E 2004 *Studies in Surface Science and Catalysis—Fischer–Tropsch Technology* vol 152 (Amsterdam: Elsevier)
[2] Anderson R B 1984 *The Fischer–Tropsch Synthesis* (Orlando, FL: Academic)
[3] Schulz H, Schaub G, Claeys M and Riedel T 1999 *Appl. Catal.* A **186** 215
[4] Dry M E 1990 *Catal. Lett.* **7** 241
[5] Niemantsverdriet J W, van der Kraan A M, van Dijk W L and van der Baan H S 1980 *J. Phys. Chem.* **84** 3363
[6] Niemantsverdriet J W and van der Kraan A M 1981 *J. Catal.* **72** 375
[7] Herranz T, Rojas S, Pérez-Alonso F J, Ojeda M, Terreros P and Fierro J L G 2006 *J. Catal.* **243** 199
[8] Datye A K, Jin Y M, Mansker L, Motjope R T, Dlamini T H and Coville N J 2000 *Stud. Surf. Sci. Catal.* **130B** 1139
[9] Davis B H 2003 *Catal. Today* **84** 83
[10] Hägg G 1931 *Z. Phys. Chem.* B **12** 33
[11] Jack K H and Wild S A 1966 *Acta Crystallogr.* **S21** A81
[12] Senateur J P, Fruchart D and Michel A 1962 *C. R. Acad. Sci.* **255** 1615
[13] Retief J J 1999 *Powder Diffract.* **14** 130
[14] du Plessis H E, de Villiers J P R and Kruger G J 2007 *Z. Kristallogr.* **222** 211
[15] Sorescu D, Thompson D L, Hurley M M and Chabalowski C F 2002 *Phys. Rev.* B **66** 035416
[16] Bromfield T C, Curulla-Ferré D and Niemantsverdriet J W 2005 *ChemPhysChem* **6** 254
[17] Nayak S K, Nooijen M, Bernasek S L and Blaha P 2001 *J. Phys. Chem.* B **105** 164
[18] Curulle-Ferré D, Govender A, Bromfield T C and Niemantsverdriet J W 2006 *J. Phys. Chem.* B **110** 13897
[19] Sorescu D 2005 *Catal. Today* **105** 44
[20] Sorescu D 2006 *Phys. Rev.* B **73** 155420
[21] Lo J M H and Ziegler T 2007 *J. Phys. Chem.* C **111** 11012
[22] Lee G D, Han S, Yu J and Ihm J 2002 *Phys. Rev.* B **66** 081403(R)
[23] Jiang D E and Carter E A 2005 *Phys. Rev.* B **71** 045402
[24] Eder M, Terakura K and Hafner J 2001 *Phys. Rev.* B **64** 115426
[25] Jiang D E and Carter E A 2004 *Surf. Sci.* **570** 167
[26] Jiang D E and Carter E A 2003 *Surf. Sci.* **547** 85
[27] Huo C-F, Li Y-W, Wang J and Jiao H 2005 *J. Phys. Chem.* B **109** 14160
[28] Chen Y-H, Cao D-B, Jun Y, Li Y-W, Wang J and Jiao H 2004 *Chem. Phys. Lett.* **400** 35
[29] Huo C-F, Ren J, Li Y-W, Wang J and Jiao H 2007 *J. Catal.* **249** 174
[30] Jiang D E and Carter E A 2003 *Phys. Rev.* B **67** 214103
[31] Jiang D E and Carter E A 2004 *Phys. Rev.* B **70** 064102
[32] Cao D-B, Zhang F-Q, Li Y-W and Jiao H 2004 *J. Phys. Chem.* **108** 9094
[33] Cao D-B, Zhang F-Q, Li Y-W, Wang J and Jiao H 2005 *J. Phys. Chem.* **109** 833
[34] Cao D-B, Zhang F-Q, Li Y-W, Wang J and Jiao H 2005 *J. Phys. Chem.* **109** 10922
[35] Cao D-B, Wang S-G, Li Y-W, Wang J and Jiao H 2007 *J. Mol. Catal.* A **272** 275
[36] Faraoun H I, Zhang Y D, Esling C and Aourag H 2006 *J. Appl. Phys.* **99** 093508
[37] Chiou W C and Carter E A 2003 *Surf. Sci.* **530** 87
[38] Liao X-Y, Cao D-B, Wang S-G, Ma Z-Y, Li Y-W, Wang J and Jiao H 2007 *J. Mol. Catal.* A **269** 169
[39] Segall M D, Lindan P J D, Probert M J, Pickard C J, Hasnip P J, Clark S J and Payne M C 2002 *J. Phys.: Condens. Matter* **14** 2717
[40] Monkhorst H J and Pack J D 1976 *Phys. Rev.* B **13** 5188
[41] Perdew J P, Chevary J A, Vosko S H, Jackson K A, Pederson M R, Singh D J and Fiolhais C 1992 *Phys. Rev.* B **46** 6671
[42] Perdew J P, Burke K and Ernzerhof M 1996 *Phys. Rev. Lett.* **77** 3865
[43] Hammer B, Hansen L B and Nørskov J K 1999 *Phys. Rev.* B **59** 7413
[44] Vanderbilt D 1990 *Phys. Rev.* B **41** 7892
[45] Hofer L J E and Cohn E M 1959 *J. Am. Chem. Soc.* **81** 1576
[46] Boettger J C 1994 *Phys. Rev.* B **49** 16798